Time-dependent incipient plasticity in Ni_3Al as observed in nanoindentation

P.C. Wo, L. Zuo, and A.H.W. Ngan[a)]
Department of Mechanical Engineering, The University of Hong Kong, Hong Kong, People's Republic of China

(Received 15 August 2004; accepted 10 November 2004)

The time-dependent characteristics of incipient plasticity in Ni_3Al during nanoindentation in the subcritical load regime were investigated statistically. The waiting time for incipient plasticity to occur at constant load was found to follow a Poisson-like distribution, with the peak shifting toward zero holding time as the load increased and eventually becoming an exponential distribution when the load was close to a critical value. The observed distribution of the strain burst waiting time at loads smaller than the critical value was inconsistent with the picture in which dislocations nucleated homogeneously out of the perfect crystal. The kinetics for the occurrence of strain burst in this case is thought to be governed by the accumulative growth of nucleation precursors.

I. INTRODUCTION

During nanoindentation, the onset of plasticity in a defect-free crystal is often associated with a sharp excursion in the indenter displacement when the load reaches a critical value, and this phenomenon is known as strain burst or pop-in.[1–4] The occurrence of a strain burst is generally believed to be the result of the generation and fast multiplication of dense dislocation structures, marking the transition from elastic to plastic deformation overall.[4–8] In constant ramping load experiments, the critical pop-in load was observed to increase with the loading rate.[9] Moreover, it was also found that a strain burst may also occur when the indentation load is held below the critical value, after a certain waiting time.[4,7] Figure 1 shows the load and displacement versus time during a nanoindentation test on a well-annealed Ni_3Al crystal. After the load was held at about 397 μN for about 18 s, a sudden increase in the displacement and a sudden drop in the load were observed simultaneously, indicating a strain burst in the specimen. In previous studies of this time-delay effects of pop-in by Gerberich et al.[7] and Chiu and Ngan,[4] the waiting time before pop-in was observed to be longer as the indentation load decreased. The statistical scatter of the results also appeared to be larger as the load decreased, but the sample sizes used in these studies, typically 5 indentations at each condition, were too small to allow convincing statistical comparison. The aim of the present study was therefore to investigate the statistical distribution of the waiting time before a pop-in occur at constant subcritical loads, with a goal of providing information on the mechanism of the delayed type of pop-in.

II. EXPERIMENTAL

An ingot was prepared by melting pure Ni (>99.92%) and Al (>99.79%) in an induction furnace, which was then homogenized in a vacuum better than 10^{-5} mbar at 1200 °C for 120 h. A disk approximately 1 mm thick and 3 mm in diameter was cut from the ingot. Both sides of the disk were mechanically polished down to 1 μm. After that, one side of the disk was coated with lacquer, and the other side was electropolished in an electrolyte of 10% perchloric acid in methanol. The side protected by lacquer was then glued onto a flat nickel block for subsequent nanoindentation tests on the electropolished side.

The composition of the ingot was determined to be $Ni_{76}Al_{24}$ by energy-dispersive x-ray analysis. Previous transmission electron microscopy observations on samples under the same heat treatment showed that the average residual dislocation spacing was greater than 20 μm.[8] As the indents made on the sample were mostly smaller than 0.5 μm in the present work, the probability of indenting on preexisting dislocation networks is very small.

Nanoindentation tests were carried out at room temperature using a Hysition Triboscope transducer (Hysitron, Minneapolis, MN) mounted on a Thermomicroscopes CP scanning probe microscope (ThermoMicroscopes, Sunnyvale, CA). A Berkovich diamond indenter was used. The tip radius of the indenter was previously

a)Address all correspondence to this author.
e-mail: hwngan@hku.hk
DOI: 10.1557/JMR.2005.0056

found to be about 500 nm using direct atomic force microscopy imaging of the tip, as well as fitting of the elastic load–displacement curve to the Hertzian contact theory.[3]

All the indentation tests were performed on one selected grain with large sectional dimensions on the free surface, to remove orientation effects. The orientation of the grain was determined to be [–0.37, 0.91, 0.18] using backscattered electron diffraction in a Cambridge Stereoscan 360 scanning electron microscope (SEM; Cambridge, UK). Thermal drift was controlled at an average rate of less than 0.5 nms^{-1}. In the nanoindentation tests, the load was first increased linearly at a rate of 1000 μNs^{-1} to 10% of the maximum load P_{max} and was then held for 10 s before ramping further at the same rate to P_{max}. The load was then held at P_{max} for a period of time before unloading linearly at 1000 μNs^{-1}. Previous observations[3] indicate that a passive oxide film on Ni_3Al would result in no significant change in the strain burst load in this material. For this reason, no special attention was paid in this work to investigate the effects of surface oxide film on the nanoindentation responses.

III. RESULTS

From the results of 30 indentation tests with 1000 μN P_{max} on the selected grain, the critical load for instantaneous pop-in, at the chosen loading rate of 1000 μNs^{-1}, was observed to be in the range 687.58 ± 51.79 μN. The delayed type of pop-in was investigated at four subcritical loads, namely, 300, 350, 400, and 500 μN. When P_{max} was lower than 500 μN, a pop-in was always observed during the load hold at P_{max}, but not earlier during the loading process, whereas when the maximum load was 500 μN, a pop-in might occur slightly before reaching P_{max}, or after reaching P_{max} during the load hold process.

More than 50 indentation data were collected at each load. Figure 2 shows a SEM image of a typical indentation array at loads between 600 to 1000 μN; the larger indents were made with 5000 μN, and they served as markers for the SEM observation. The indentations were made at more than 10 μm away from any grain boundary segments and the indents were at least 5 μm away from each other, so that deformation around individual indentations would not interfere with each other.

The waiting time t_{exc} before the occurrence of pop-in, and the corresponding length of excursion h_{exc} in the indenter displacement were recorded for each load. Figure 3 shows a plot of t_{exc} and h_{exc} against the indentation load. Each data point for loads between 300 and 500 μN represents an average of more than 50 indentations. The results at 600 and 700 μN were the average of 5 indentation tests. It is observed from Fig. 3 that at a

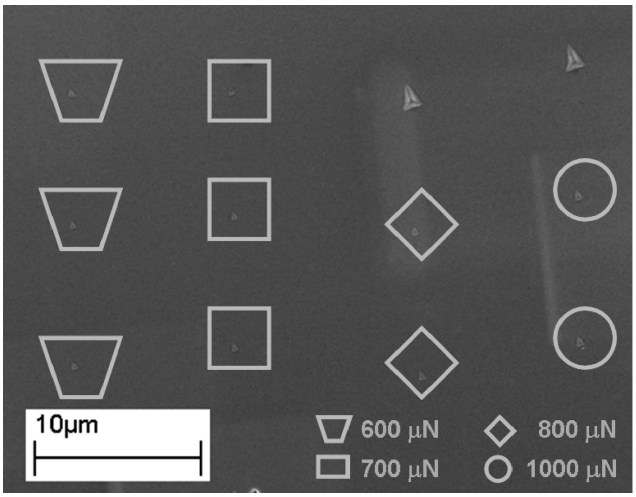

FIG. 2. SEM image of a typical array of indents made with loads between 600 and 1000 μN. The larger indents are made with 5000 μN, which served as markers only.

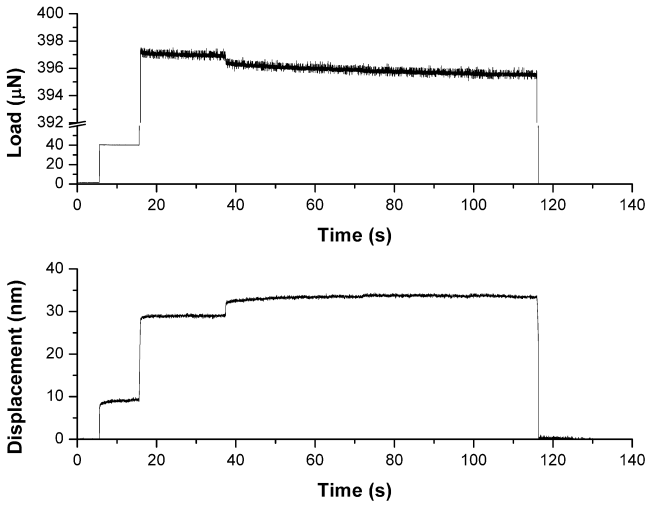

FIG. 1. Load and displacement versus time during a constant-load indentation experiment in a well-annealed Ni_3Al crystal.

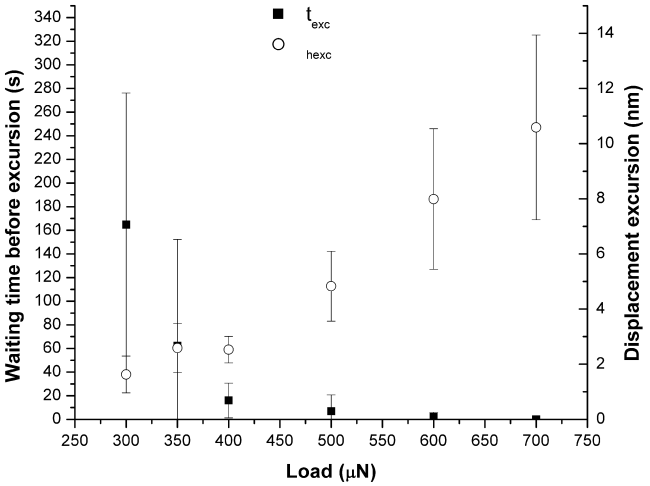

FIG. 3. Waiting time before strain burst and the corresponding excursion in the indentation depth versus the normal load.

lower load, it takes a longer waiting time to exhibit a pop-in, but the statistical dispersion of t_{exc} also increases at lower loads. These results are very similar to those observed by Chiu and Ngan in a similar study on Ni_3Al [111] single crystal,[4] albeit the much larger sample sizes in the present work.

Figures 4(a)–4(d) show the probability distributions for the pop-in waiting time at 300, 350, 400, and 500 μN, respectively. Two types of distributions are observed: (i) peaked, Poisson-like distributions for 300, 350 and 400 μN, and (ii) exponential distribution for 500 μN. A close inspection of the Poisson-like distributions at 300 to 400 μN in Figs. 4(a)–4(c), reveals a shifting of peak from 5–10 s at 400 μN to 75–125 s at 300 μN, i.e., the modal waiting time is longer at lower loads. At 300 and 350 μN, the distribution appears to be bimodal with a lower peak at a longer waiting time. The bimodal shape is less obvious at higher loads.

IV. DISCUSSION

A. Review of proposed mechanisms of incipient plasticity

At present, there is no generally accepted explanation for the delay in the occurrence of strain burst at subcritical loads. Also, different materials may have different reasons for exhibiting the delayed type of strain burst. One mechanism put forward earlier by the present authors may be described as the "invisible defect" theory.[4,8] In this mechanism, the application of a subcritical load is assumed to cause the instantaneous formation of some stable defect, which would be unzipped due to the strong image force if the load is removed, hence the term "invisible defect" and the observation that the material would seem to recover elastically upon load removal. However, if the load is held for some time at a subcritical value, the invisible defect may grow by, for example, climb, and when it reaches the critical unstable size, an avalanche event would occur and a strain burst would result. Two factors would contribute to significant diffusion underneath a nanoindent even at a low homologous temperature such as room temperature.[4,10] First, the diffusion path involved is very short, as the typical distance from the nearest free surface to the core of the indent is usually submicron in the case of nanoindentation. Secondly, the stress gradient involved in nanoindentation is typically several gigapascal per micrometer, which is many orders of magnitude higher than the usual megapascal per micrometer in bulk creep. The large stress gradient in nanoindentation gives rise to a large chemical potential gradient which is the driving force for diffusion. Recent computer simulations on nanoindentation of Cu along the [001] orientation indicate the existence of a special form of invisible defects, namely, Lomer–Cottrell

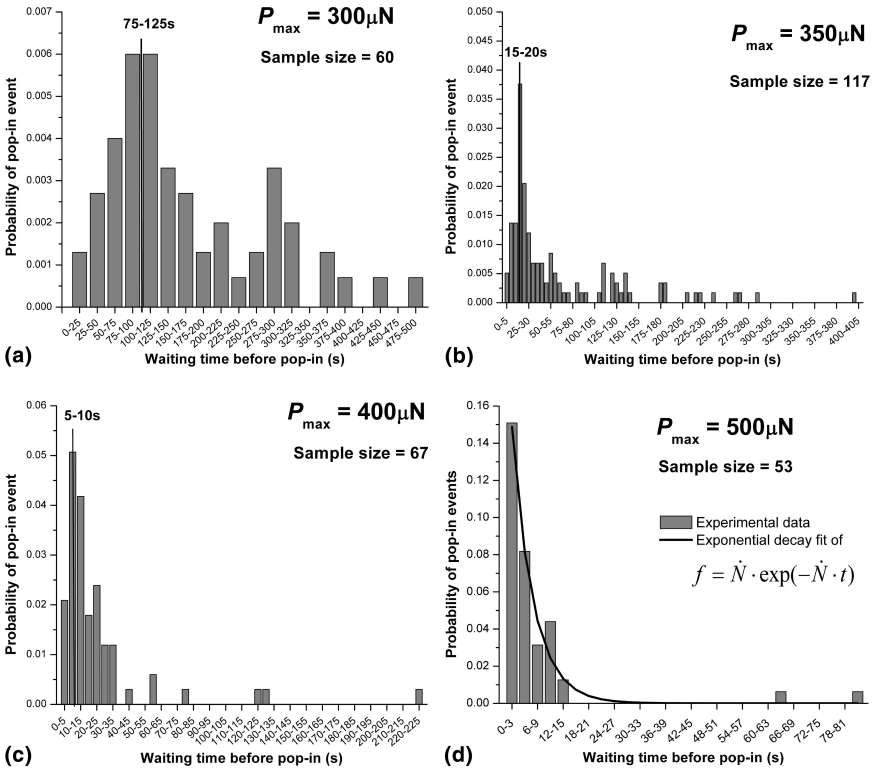

FIG. 4. Probability histogram for the waiting time of pop-in at indentation load of (a) 300 μN, (b) 350 μN, (c) 400 μN, and (d) 500 μN. An exponential fit using the values of υ^* and η obtained from Fig. 5 is superimposed in (d).

locks, which are unzipped when the load is removed.[11] However, the Lomer–Cottrell locks are not generally observed in other loading orientations.

On the other hand, Schuh and Lund[9] recently studied the distribution of the critical pop-in loads under constant loading rate conditions in SiC, and concluded that the observed statistics obey the characteristics of a mechanism involving thermally activated, stress-assisted homogeneous nucleation of dislocations. In this model, the nucleation rate of unstable dislocation loops in a virgin sample at any time depends only on the instantaneous load, but is independent of the load history of the sample. In a large number of samples, the cumulative frequency $F(t)$ of the samples exhibiting a life (the pop-in waiting time) longer than t is given by

$$\frac{dF(t)}{dt} = -\dot{N}(\tau)\, F(t) \quad , \tag{1}$$

where $\dot{N}$ is the nucleation rate which in Schuh and Lund's work is assumed to depend on the instantaneous stress τ but not its history. Schuh and Lund further assumed a simple Boltzmann form for $\dot{N}$, namely, $\dot{N}(\tau) = \eta \exp(\tau\upsilon^*/kT)$, where η represents the nucleation rate in a stress-free crystal due to thermal activation alone, υ^* is the activation volume, and kT is the thermal energy. In a constant loading rate test, τ is a linear function of t, and so Eq. (1) can be integrated to give

$$F(\tau) = \exp\left[-\frac{\eta kT}{\dot{\tau}\upsilon^*}\exp\left(\frac{\tau\upsilon^*}{kT}\right)\right] \quad , \tag{2}$$

where $\dot{\tau}$ is the constant loading rate. By performing constant-loading-rate tests on SiC, Schuh and Lund[9] were able to obtain a distribution of the critical load τ at which spontaneous pop-in occurred, which obeys the form predicted in Eq. (2). The activation volume of defect formation they calculated from their results however, is on the order of atomic volume, instead of the volume expected from a dislocation loop.

In their paper, Schuh and Lund[9] limited the application of their homogeneous nucleation model to critical load situations under constant loading rates in SiC. Note, however, that when applied to the present context for the delayed type of pop-in observed in Ni_3Al under constant subcritical loads, the implication of the homogeneous nucleation model would be intrinsically inconsistent with that of the "invisible defect" model described above. In the homogeneous nucleation model, a "virgin" sample is defined as one in which pop-in has not occurred, and for such a sample, the chance that a pop-in will occur in the next unit time does not depend on how long the (subcritical) load has already been applied on the sample. In the invisible defect model, a sample that has been loaded subcritically for a longer time would have a higher chance to exhibit a pop-in in the next unit time because the invisible defect would have climbed to a larger size and therefore be closer to criticality.

B. Interpretation of the present results

1. Homogeneous nucleation at 500 μN and above

The present data at 500 μN in Fig. 4(d) evidently obey an exponential distribution. An exponential distribution of the sample life (pop-in time) is consistent with the homogeneous nucleation picture proposed by Schuh and Lund.[9] This can be seen easily from Eq. (1). If load τ is constant, the nucleation rate $\dot{N}$ would also be constant, and hence the solution to Eq. (1) is the exponential decay function $F(t) = \exp(-\dot{N}t)$. Note that $F(t)$ is the cumulative frequency of samples with life longer than t; the relative frequency distribution function $f(t)$ of sample life t is related to it by $F(t) = \int_t^\infty f(t')dt'$, or $f = -dF/dt$. Hence, $f(t)$ would also be exponential decaying with the same time constant as F. The exponential distribution of the pop-in times at 500 μN in Fig. 4(d) therefore suggests that the delay in pop-in at this load is due to the kinetics involved in nucleating a defect from a homogeneous site.

The time constant of the exponential decay observed in Fig. 4(d) can be related to the parameters υ^* and η in Eq. (2), but a second condition would be required to work out the individual values of υ^* and η. We therefore repeat the analysis in Schuh and Lund's paper[9] here, involving the use of the spontaneous pop-in loads observed in the experiments in which the load was ramped up to 1000 μN at a constant rate. From Eq. (2), a plot of $\ln[\ln(1/F)]$ versus τ should yield a straight line with slope equal to υ^*/kT. Figure 5 shows such a plot for our data. The value of τ used here is the maximum resolved shear

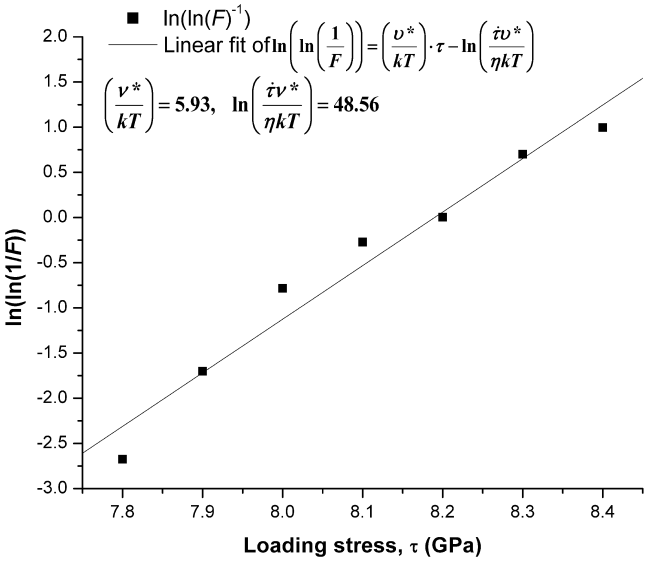

FIG. 5. Plot of $\ln[\ln(F)^{-1}]$ versus the loading stress at which a pop-in occurred. The values of υ^* and η are obtained from the slope and y-intercepts of the linear fit.

stress at the most highly stress point underneath the indenter and is equal to $0.31P_o$, where $P_o = (6PE_r{}^2/\pi^3R^2)^{1/3}$ is the maximum pressure,[12] P is the indentation load, R is the radius of the indenter tip, and E_r is the reduced modulus. Here, E_r was evaluated from the elastic constants of Ni_3Al ($C_{11} = 230$ GPa, $C_{12} = 150$ GPa, and $C_{44} = 131$ GPa[13]) and the known reduced modulus of the diamond tip (1140 GPa), using the method by Vlassak and Nix.[14] The value of υ^* derived from the slope of the fitted line in Fig. 5 is 2.45×10^{-2} nm^3, whereas the value of η calculated from the y intercept is 4.61×10^{-20} s^{-1}. Using these values of υ^* and η, the nucleation rate $\dot{N}$ calculated from $\dot{N} = \eta \exp(\tau\upsilon^*/kT)$ at τ corresponding to 500 μN equals 1.4 s^{-1}. In Fig. 4(d), the exponential probability function for the 500 μN data was fitted with a function of the form $\dot{N}\exp(-\dot{N}t)$, and $\dot{N}$ was found to be around 0.2 s^{-1} from the fit. The deviation between the two estimates of $\dot{N}$ is due to the sensitivity of the nucleation rate to the value of υ^*, as its exponential value is involved in the expression of $\dot{N}$. Conversely, the value of υ^* calculated from the fitted values of 0.2 s^{-1} and 4.61×10^{-20} s^{-1} for $\dot{N}$ and η, respectively, is 2.35×10^{-2} nm^3, which is only about 4% different from the value of 2.45×10^{-2} nm^3 obtained from Fig. 5.

However, the conclusion we arrive at here leads to a similar problem encountered by Schuh and Lund.[9] That is, although the small order of magnitude for the value of η is reasonable, since it suggests the impossibility of defect generation in a stress-free crystal due to thermal activation alone, the atomic scale of the activation volume is much smaller than the volume expected from a dislocation loop. Although Schuh and Lund suggested that this might be due to the aggregation of point defects with the same activation energy or the growth of dislocation loop from an atomic-size region, the details of these have not been made clear yet.

To gain some insight into the nature of the homogeneous nucleation process at high stresses, we have performed molecular dynamics simulations. We used the atomic potentials for Ni_3Al developed by Voter and Chen.[13] The full-scale nanoindentation geometry comparable to experimental conditions is too large to simulate, so instead, we simulated a small block of perfect crystal under a high shear stress, representing the most highly stressed region in the sample underneath the indenter tip. This block had an array of $36 \times 36 \times 24$ atoms or $4.5 \times 7.4 \times 10.5$ nm, along the three crystallographic directions of $[10\bar{1}]$, [111], and $[1\bar{2}1]$, respectively. Periodic boundary conditions were used along the $[10\bar{1}]$ and $[1\bar{2}1]$ directions, and the (111) surface was left free. The simulation temperature was controlled at 300 K using a Woodcock thermostat.[15] A constant strain rate of 5×10^8 s^{-1} was applied by keeping the lowest (111) layer fixed throughout the simulation and giving an initial velocity along the $[10\bar{1}]$ direction to the topmost (111) layer. To avoid a shock wave, a linearly interpolated velocity profile was also given initially to the remaining layers between the bottom and the topmost layers.[16] The onset of crystal plasticity was detected by looking for a jump in the simulated stress–strain curve. The nuclei for instability were identified by plotting only atoms with high enough energies or relative displacements with respect to neighbors.[17] Figure 6 shows a series of snapshots during an instability event. The outcome of the instability is the generation of slip near the middle (111) plane of the simulation cell. As shown in Figs. 6(b)–6(e), this took place via the generation and expansion of a dislocation loop, which was identified to be a Shockley partial dislocation loop with Burgers vector $1/6[1\bar{2}1]$. The Shockley partial loop bounded a complex stacking fault and was quickly attracted to the periodic cell boundaries to annihilate with its images as shown in Figs. 6(d)–6(e). The eventual expansion and annihilation of the partial loop and the associated widespread faulting of the crystal are not realistic due to the periodic boundaries. However, what is interesting here is that in the very early stage, the loop developed from a small cluster composing of only a few atoms, as shown in Figs. 6(a)–6(c). This cluster was not a vacancy but was simply a few atoms with momentarily higher-than-average thermal vibrations, i.e., a "hot spot" in the crystal. The life times of these hot spots were only typically about 10 cycles of simulation time steps, corresponding to around 60 fs in real time, and most hot spots annihilated before developing into dislocation loops. Thus, although the subsequent developments in Figs. 6(d) and 6(e) are not realistic, the initial processes shown in Figs. 6(a)–6(c) suggest that the simulated hot spots are likely to be the atomic-sized nuclei deduced from the distribution of the critical pop-in loads in Fig. 4. It is important to note that the simulations here are meant to provide information on how homogeneous nucleation occurs in Ni_3Al alone, and since dislocation mechanisms in other materials may be different, one cannot simply presume that the mechanism observed in the simulations here will occur in other materials.

2. Incipient plasticity at lower extra loads

The peaked distributions at 400 μN and below as shown in Figs. 4(a)–4(c) clearly do not obey the exponential form expected from Eq. (1) by assuming $\dot{N}$ to be constant, and hence the conclusion must be that at smaller loads, the delay in pop-in is not due to homogeneous nucleation. Apparently, at small stresses, homogeneous nucleation is too slow, and some other mechanism takes over.

The invisible defect mechanism remains a possible explanation. To explain the peaked distributions in Figs. 4(a)–4(c), we propose here that the invisible defects

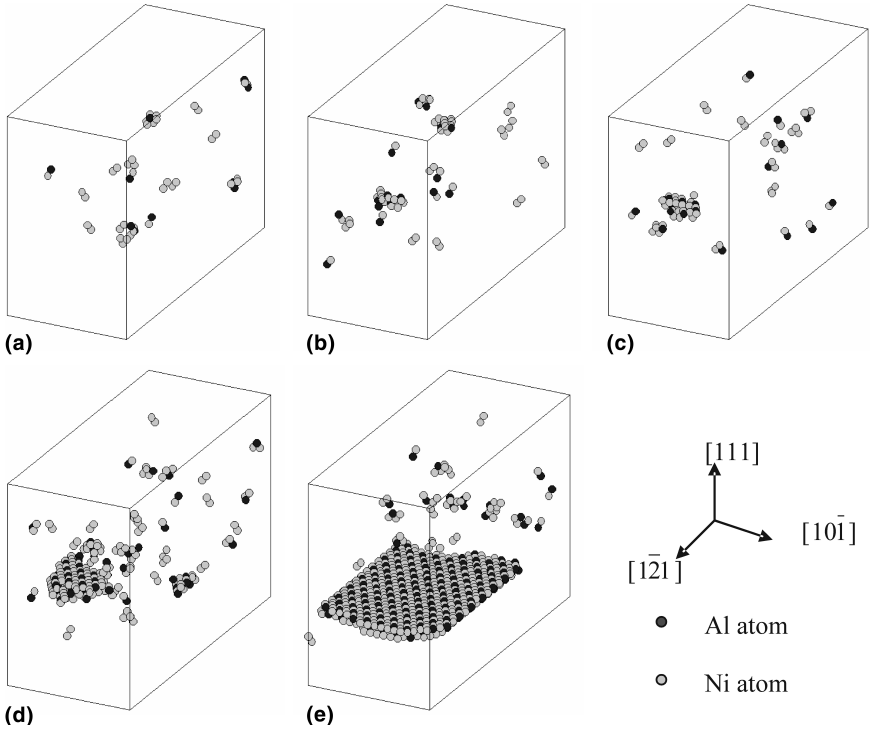

FIG. 6. Molecular dynamics simulation of the microstructure evolution at the most highly stressed point in a perfect crystal under the indenter tip during an instability event. (a) A block of perfect crystal is elastically sheared along [10$\bar{1}$]. (b) Small clusters of a few energetic atoms appear within the crystal. (c) A Shockley partial loop (b = 1/6[1$\bar{2}$1]) is generated from an atom cluster. (d,e) The expansion of this Shockley partial loop.

are a form of precursors to the nucleation of unstable dislocation loops. These nucleation precursors could be single vacancies or clusters of them, or simply hot spots of the form shown in Fig. 6 but with greatly extended life times. Another possible origin of these precursors may be steps or roughness on the sample surface, which may cause high enough stress concentrations in the neighborhood to result in more rapid vacancy transport, for example. Unfortunately, the kinetics involved in the low stress regime is too slow to be directly simulated by finite-temperature molecular dynamics, so the details of these nucleation precursors cannot be revealed. Whatever they may be, their activation volumes are assumed to be small so that their formation or growth would not lead to detectable changes in the indenter tip displacement, hence they are invisible. However, once formed, they may act during their life times as heterogeneous sites for nucleation of unstable dislocation loops. We further propose that these precursors become more numerous, or grow to larger sizes, as the time under load increases; i.e., we assume a history-dependent, damage accumulation model. The effect is that the nucleation rate $\dot{N}$ in Eq. (1) is not a constant at constant stress conditions, but is an increasing function of time. The general solution to Eq. (1) can be written as

$$F(t) = \exp\left[-\int_0^t \dot{N}(t')\mathrm{d}t'\right] \quad . \tag{3}$$

The frequency distribution function $f(t)$ of the pop-in times of the samples is therefore

$$f(t) = -\frac{\mathrm{d}F}{\mathrm{d}t} = \dot{N}(t)\,\exp\left[-\int_0^t \dot{N}(t')\,\mathrm{d}t'\right] \quad . \tag{4}$$

Since we assume $\dot{N}(t)$ to increase with t, and clearly the exponential term in Eq. (4) is decreasing with t, $f(t)$ is therefore a peaked function with an exponential tail, as observed experimentally in Figs. 4(a)–4(c).

It is likely that $\dot{N}(t)$ has a Boltzmann form with an activation energy decreasing with time and an activation volume increasing with time. However, we do not know the exact nature of the nucleation precursors so $\dot{N}(t)$ cannot be derived theoretically. On the other hand, from Eqs. (3) and (4), the function $\dot{N}(t)$ can be evaluated from the experimental frequency distributions in Figs. 4(a)–4(d) as

$$\dot{N}(t) = \frac{f(t)}{\sum_{t' \geq t} f(t')\,\Delta t} \quad , \tag{5}$$

where Δt is the time interval in the frequency distributions. Figure 7 shows the calculated nucleation rate versus time at different indentation loads, using the data in Fig. 4. As it is mentioned above, $\dot{N}(t)$ is likely to have a Boltzmann form, and so it would be more convenient to plot $\ln\dot{N}$ versus time at different indentation loads, as

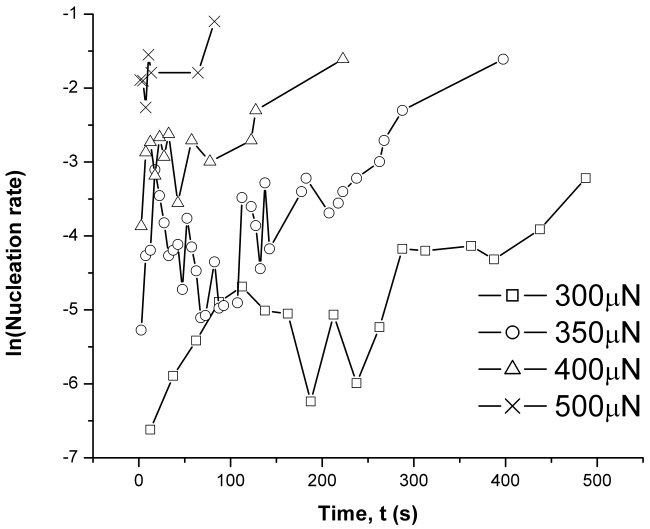

FIG. 7. Plot of $\ln[\dot{N}(t)]$ versus time at 300, 350, 400, and 500 μN.

shown in Fig. 7. It is observed that, at constant loads of 300, 350, and 400 μN, $\dot{N}(t)$ increases nearly exponentially with time, suggesting that the activation energy decreases nearly linearly with time, which agrees with the postulation of a damage accumulation model that we put forward above. Also, at a particular time t, the nucleation rate is higher at a higher load. This corresponds to the experimental observation in Fig. 3 that a shorter holding time is required for the occurrence of pop-in at higher loads. From Fig. 7, the nucleation rate at 500 μN appears to be the upper limit as load increases, and in our nucleation precursor model proposed above, this upper limit corresponds to the scenario in which the nucleation precursors become so small that they are no different from the nuclei themselves. At 500 μN or higher, the nucleation process is no longer required to go through the precursor process and hence becomes homogeneous.

V. CONCLUSIONS

The statistics of delays in pop-in event during constant-load nanoindentation were studied in Ni_3Al. The occurrence of pop-in in the subcritical load regime was found to depend on the load history, such that at a smaller load, a longer hold time is required for a pop-in to occur. This behavior cannot be explained by the homogeneous nucleation of defects alone. To explain the results, the multiplication and growth of stable or metastable defects, which act as nucleation precursors to unstable defects, are proposed to be involved in the nucleation of the incipient plasticity process.

At or near the critical load, however, the results indicate homogeneous nucleation with atomic sized nuclei. Molecular dynamics simulations suggest that these homogeneous nuclei are likely to be hot atomic clusters with limited lifetimes in the crystal.

ACKNOWLEDGMENT

The work described in this paper was supported by grants from the Research Grants Council of the Hong Kong Special Administrative Region, People's Republic of China (Project No. HKU7062/01E, HKU7201/03E).

REFERENCES

1. S.A. Syed Asif and J.B. Pethica: Nanoindentation creep of single-crystal tungsten and gallium arsenide. *Philos. Mag. A* **76,** 1105 (1997).
2. W.W. Gerberich, J.C. Nelson, E.T. Lilleodden, R. Anderson, and J.T. Wyrobek: Indentation induced dislocation nucleation: The initial yield point. *Acta Mater.* **44,** 3585 (1996).
3. Y.L. Chiu and A.H.W. Ngan: Time-dependent characteristics of incipient plasticity in nanoindentation of a Ni_3Al single crystal. *Acta Mater.* **50,** 1599 (2002).
4. Y.L. Chiu and A.H.W. Ngan: A TEM investigation on indentation plastic zones in Ni_3Al (Cr, B) single crystals. *Acta Mater.* **50,** 2677 (2002).
5. C.F. Robertson and M.C. Fivel: A study of the submicron intent-induced plastic deformation. *J. Mater. Res.* **14,** 2251 (1999).
6. J. Li, A.H.W. Ngan, and P. Gumbsch: Atomic modelling of mechanical behaviour. *Acta Mater.* **51,** 5711 (2003).
7. W.W. Gerberich, S.K. Venkataraman, H. Huang, S.E. Harvey, and D.L. Kohlstedt: The injection of plasticity by millinewton contacts. *Acta Mater.* **43,** 1569 (1995).
8. P.C. Wo and A.H.W. Ngan: Incipient plasticity during nano-scratch in Ni_3Al. *Philos. Mag.* **84,** 3145 (2004).
9. C.A. Schuh and A.C. Lund: Application of nucleation theory to the rate dependence of incipient plasticity during nanoindentation. *J. Mater. Res.* **19,** 2152 (2004).
10. H. Li and A.H.W. Ngan: Size effects of nanoindentation creep. *J. Mater. Res.* **19,** 513 (2004).
11. H.Y. Liang, C.H. Woo, H. Huang, A.H.W. Ngan, and T.X. Yu: Dislocation nucleation in the initial stage during nanoindentation. *Philos. Mag.* **83,** 3609 (2003).
12. K.L. Johnson: *Contact Mechanics* (Cambridge Univ. Press, Cambridge, U.K., 1987), p. 93.
13. A.F. Voter and S.P. Chen: In *Characterization of Defects in Materials,* edited by R.W. Siegel, J.R. Weertman, and R. Sinclair (Mater. Res. Soc. Symp. Proc. **82,** Pittsburgh, PA, 1987), p. 175.
14. J.J. Vlassak and W.D. Nix: Measuring the elastic properties of anisotropic materials by means of indentation experiments. *J. Mech. Phys. Solids* **42,** 1223 (1994).
15. L.V. Woodcock: Isothermal molecular dynamics calculations for liquid salts chem. *Phys. Lett.* **10,** 257 (1970).
16. M.F. Horstemeyer, M.I. Baskes, and S.T. Plimpton: Length scale and time scale effects on the plastic flow of fcc metals. *Acta Mater.* **49,** 4363 (2001).
17. A.H.W. Ngan, M. Wen, and C.H. Woo: Atomistic simulation of Paidar-Pope-Vitek lock formation in Ni_3Al. *Comput. Mater. Sci.* **29,** 259 (2004).